

Rethinking Video Salient Object Ranking

Jiaying Lin, Huankang Guan and Rynson W.H. Lau[†]

Department of Computer Science, City University of Hong Kong, Hong Kong
Emails: {jiayinlin5-c, huankang.guan}@my.cityu.edu.hk, Rynson.Lau@cityu.edu.hk

[†] Rynson W.H. Lau is the corresponding author.

Abstract

Salient Object Ranking (SOR) involves ranking the degree of saliency of multiple salient objects in an input image. Most recently, a method is proposed for ranking salient objects in an input video based on a predicted fixation map. It relies solely on the density of the fixations within the salient objects to infer their saliency ranks, which is incompatible with human perception of saliency ranking. In this work, we propose to explicitly learn the spatial and temporal relations between different salient objects to produce the saliency ranks. To this end, we propose an end-to-end method for video salient object ranking (VSOR), with two novel modules: an intra-frame adaptive relation (IAR) module to learn the spatial relation among the salient objects in the same frame locally and globally, and an inter-frame dynamic relation (IDR) module to model the temporal relation of saliency across different frames. In addition, to address the limited video types (just sports and movies) and scene diversity in the existing VSOR dataset, we propose a new dataset that covers different video types and diverse scenes on a large scale. Experimental results demonstrate that our method outperforms state-of-the-art methods in relevant fields. We will make the source code and our proposed dataset available.

Keywords: Video Salient Object Ranking, Saliency Ranking, Salient Object Detection

1 Introduction

Salient Object Ranking (SOR) is a task that aims to rank salient objects according to their degrees of visual saliency. In recent years, SOR is beginning to attract some research attention [Liu, Li, Zhao, Han, and Shao \(2021\)](#); [Siris, Jiao, Tam, Xie, and Lau \(2020\)](#); [Z. Wang, Yan, Han, and Sun \(2019\)](#), as it provides insights into how the human visual system works. SOR also has some potential downstream applications, including image captioning [Yao, Pan, Li, and Mei \(2018\)](#), image cropping [Liu et al. \(2021\)](#) and compression [Z. Li, Qin, and Itti \(2011\)](#). However, majority of the SOR works focus only on static images, and SOR on videos is still under exploration. Compared with

SOR on static images, video salient object ranking (VSOR) is more challenging since the saliency degree of each object may change over time, and is further complicated by the dynamic human attention characteristics like selective attention and attention shift [Fan, Wang, Cheng, and Shen \(2019\)](#); [Koch and Ullman \(1987\)](#); [W. Wang et al. \(2019\)](#).

Recently, Wang *et al.* [Z. Wang et al. \(2019\)](#) propose the first VSOR method (named SVSNet) with a new dataset. They use the ratio of the number of eye fixation points landed on each object to infer the relative saliency rank among the objects, and propose a fixation-based VSOR method. However, their solution has multiple limitations. First, it relies solely on the density of eye fixations to

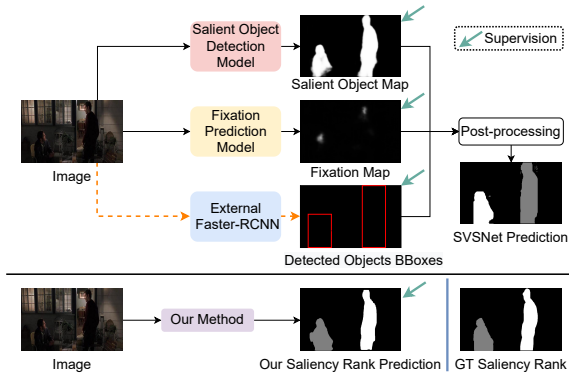


Fig. 1: Differences between SVSNet [Z. Wang et al. \(2019\)](#) (top) and our proposed framework (bottom). As SVSNet [Z. Wang et al. \(2019\)](#) depends heavily on the predicted eye-fixation and constrains their rank masks in bounding boxes, it is unreliable for inferring the saliency rank and leads to unnatural boundaries in its output masks. In contrast, our end-to-end framework for VSOR can precisely predict the saliency rank without any post-processing nor eye fixation supervision.

establish the GT saliency ranks for their proposed dataset, which is incompatible with human perception [Siris et al. \(2020\)](#) that the order of fixation points (scanpath) reflects the object saliency ranks. In addition, it also requires the eye fixation supervision. However, ground truth eye-fixation maps are generally not available. Second, it uses an external object detector to detect every object in the input image. While the detected objects may not necessarily be salient, their method also lacks the ability to model the saliency correlation among different objects as the detected object features from the external object detector is not used in the training process. Third, as it can only differentiate different objects in terms of bounding boxes rather than at pixel-level, its output masks typically have unnatural boundaries. Fourth, their proposed dataset uses the density of fixation points inside each object to determine the ground truth saliency ranks. Such an approach leads to missing salient objects in the final output, which will be discussed in [Section 3](#). These limitations motivate us to develop a new method and a new dataset with more accurate saliency rank annotations to address the VSOR problem.

To tackle the above problems, we observe that the saliency degree of each salient object is determined by the spatial information of a static image at the intra-frame level, and is affected by the temporal information (such as motion) at the inter-frame level. Hence, in this paper, we propose a novel end-to-end approach to rank salient objects in videos, with two novel modules. We first propose an Intra-frame Adaptive Relation (IAR) module to adaptively learn the spatial saliency degrees among different objects in each frame. We then propose an inter-frame Dynamic Relation (IDR) module to dynamically model the temporal saliency across different frames. [Figure 1](#) shows the superiority of the proposed approach. Although our method does not require any post-processing nor eye fixation supervision, it can still detect the saliency ranks correctly. Besides, the RVSOD dataset proposed by [Wang et al. Z. Wang et al. \(2019\)](#) contains mainly sports videos and movies [Mathe and Sminchisescu \(2014\)](#). Over 80% of eye-fixations in RVSOD fall onto humans, while other types of objects are rarely detected. Some of the videos from RVSOD only contain a single salient object (*i.e.*, no saliency ranks). These limitations significantly constrain the robustness of the trained model. In this work, we propose a new challenging VSOR dataset that covers a wide range of scenes and salient object categories. It contains a total of 128 videos with 17,584 video frames and corresponding annotated saliency rank masks. Each video in our dataset has at least two salient objects with saliency ranks. We have conducted extensive experiments to evaluate our method and show that the proposed method outperforms state-of-the-art methods on both RVSOD and our proposed datasets.

The main contributions of our work include:

- We propose the first end-to-end method for video salient object ranking, which does not require eye-fixation labels for supervision nor any post-processing to infer the saliency ranks. It consists of an Intra-frame Adaptive Relation (IAR) module and an inter-frame Dynamic Relation (IDR) module to model the spatial and temporal correlations among the salient objects in the same frame and across frames, respectively.
- We propose a challenging large-scale VSOR dataset with 128 videos of different types and

17,584 video frames containing a variety of salient objects from diverse scenes.

- Extensive experiments show superior performances of our method on both RVSOD and our proposed datasets, compared with other state-of-the-art methods from related fields.

2 Related Work

2.1 Image-based Salient Object Ranking

In [A. Islam \(2018\)](#), Salient Object Ranking (SOR) is first investigated. It aims to infer the saliency degree of objects in a single image. [Siris *et al.* \(2020\)](#) then investigate the relationship between human attention shift and the saliency rank of objects. Based on their observations, they propose a new dataset and a multi-stage method for SOR. [Liu *et al.* \(2021\)](#) further propose a graph-based SOR method to model the relative saliency among different salient objects and a refined SOR dataset based on the one constructed by [Siris *et al.* \(2020\)](#). [Fang *et al.* \(2021\)](#) utilize the position information of salient objects to design a new end-to-end SOR method.

However, these image-based SOR methods may be effective when applied to video salient object ranking, as they do not model the temporal relations of salient objects across frames.

2.2 Video-based Salient Object Ranking

Video Salient Object Ranking (VSOR) is a new research problem recently proposed by [Wang *et al.* \(2019\)](#). They construct a ranking video salient object dataset, called RVSOD, from existing dynamic eye-tracking datasets, Hollywood2 [Mathe and Sminchisescu \(2014\)](#) and UCF sports [Mathe and Sminchisescu \(2014\)](#). They also propose a multi-stage method, SVSNet, which uses salient object maps and eye fixation maps to predict the saliency rank maps in their post-processing module.

However, their constructed datasets are selected from sports videos and movies with limited diversity. Besides, their method directly produces the saliency rank maps by combining the coordinates of the bounding boxes for each object, detected salient object maps, and eye fixation

in the videos. It leads to insufficient relationship modeling between different salient objects in a feature level, and inaccurate and unstable results.

To address these limitations, in this work, we construct a new VSOR dataset with diverse videos and more accurate annotations, and propose a new fixation-free and end-to-end method for more reliable predictions of saliency ranks.

2.3 Video Salient Object Detection

Video Salient Object Detection (VSOD) has attracted much attention from researchers in recent years. Earlier methods for VSOD are mostly based on handcrafted features [Chen, Li, Wang, Qin, and Hao \(2017\)](#); [C. Guo, Ma, and Zhang \(2008\)](#); [F. Guo *et al.* \(2017\)](#), such as boundary connectivity [J. Zhang *et al.* \(2015\)](#) and gradient flow [W. Wang, Shen, and Shao \(2015\)](#). Recent VSOD methods achieve better performance with the help of deep learning [Gu *et al.* \(2020\)](#); [G. Li, Xie, Wei, Wang, and Lin \(2018\)](#); [Song, Wang, Zhao, Shen, and Lam \(2018\)](#); [W. Wang, Shen, and Shao \(2017\)](#). [Fan *et al.* \(2019\)](#) propose a large-scale dataset for VSOD and utilize attention shift and convLSTM [Xingjian *et al.* \(2015\)](#) in their method. [Ren *et al.* \(2020\)](#) propose an excitation strategy for refining the prediction of VSOD models. [Li *et al.* \(2019\)](#) exploit optical flow to generate motion guided attention for VSOD. [Zhang *et al.* \(2021\)](#) proposes a dynamic strategy of context fusion for VSOD.

All these VSOD methods cannot distinguish the relative saliency among different objects since they mainly focus on performing binary salient object prediction.

3 Dataset

Although [Wang *et al.* \(2019\)](#) propose the RVSOD dataset for VSOR, it mainly contains sports videos and movies [Mathe and Sminchisescu \(2014\)](#) with over 80% of the salient objects being humans. This limits the diversity and generality of the dataset. The left part of [Figure 2](#) shows snapshots of some videos from RVSOD. To address these limitations, we have



Fig. 2: Comparison between RVSOD [Z. Wang et al. \(2019\)](#) and our proposed DAVSOR. While RVSOD mainly includes sports videos and movies with limited number of salient objects, our dataset contains diverse video types, *e.g.*, with multiple humans, animals, vehicles and man-made objects.

constructed a large-scale video salient object ranking dataset, named **DAVSOR** (Densely Annotated Video Salient Object Ranking), which includes 17,584 video frames and corresponding masks for saliency ranking. Our proposed dataset **DAVSOR** contains videos of different categories (*e.g.*, Animals, Vehicles and Human Activities). The right part of Figure 2 shows snapshots of some videos from our proposed DAVSOR, exhibiting a much higher diversity.

3.1 Construction of the Dataset

To construct our VSOR dataset, we collect our videos and the corresponding eye-fixation maps and salient object masks from an existing video salient object detection dataset DAVSOD [Fan et al. \(2019\)](#). The videos in our dataset cover diverse categories and complex scenes, thus more challenging for VSOR (see the right part of Figure 2).

Unlike RVSOD [Z. Wang et al. \(2019\)](#), which directly generates the saliency rank from the eye-fixation maps and instance masks, we obtain the corresponding masks of the saliency rank by manually re-annotating the saliency rank from the salient instance labels provided by [Fan et al. \(2019\)](#), with careful checking. Specifically, we ask five human annotators to rank the saliency according to the corresponding fixations and salient instance annotations from [Fan et al. \(2019\)](#). After obtaining the initial saliency ranks from the human annotators, we carefully validate them to check if the saliency ranks align with the corresponding fixations and the GT salient instance annotations. Figure 3 shows the difference between the saliency ranks generated by RVSOD [W. Wang et al. \(2019\)](#) and ours. The saliency rank from our dataset is more accurate,

compared with those in RVSOD. In particular, their approach of generating the saliency ranks may cause some salient objects in RVSOD to disappear from their salient ranks.

We follow the training and test splits from [Fan et al. \(2019\)](#). Our proposed DAVSOR contains 7,403 and 10,181 video frames in the training set and test set, respectively.

3.2 Dataset Analysis

To give a better understanding of our VSOR dataset, we conduct some statistical analyses on our proposed DAVSOR. Table 1 compares between RVSOD [Z. Wang et al. \(2019\)](#) and our proposed DAVSOR. Overall, DAVSOR is larger in scale and more diverse in the numbers of video categories and salient object types. Table 2 compares the statistical distribution of salient objects between RVSOD [Z. Wang et al. \(2019\)](#) and DAVSOR. It is worth noting that RVSOD [Z. Wang et al. \(2019\)](#) has a large portion of video frames with only one salient object, which can be considered as invalid frames, leading to a high invalid rate in RVSOD for video salient object ranking. Unlike RVSOD [Z. Wang et al. \(2019\)](#), DAVSOR has no invalid video frames and is more balanced in the distribution of the number of salient objects. These analyses demonstrate the superiority of our proposed DAVSOR.

4 Method

In this paper, we propose a novel end-to-end video salient object ranking (VSOR) method. Figure 4 illustrates the pipeline. For each input video frame, we first feed it to the backbone feature extraction network ResNet-50 [He, Zhang,](#)

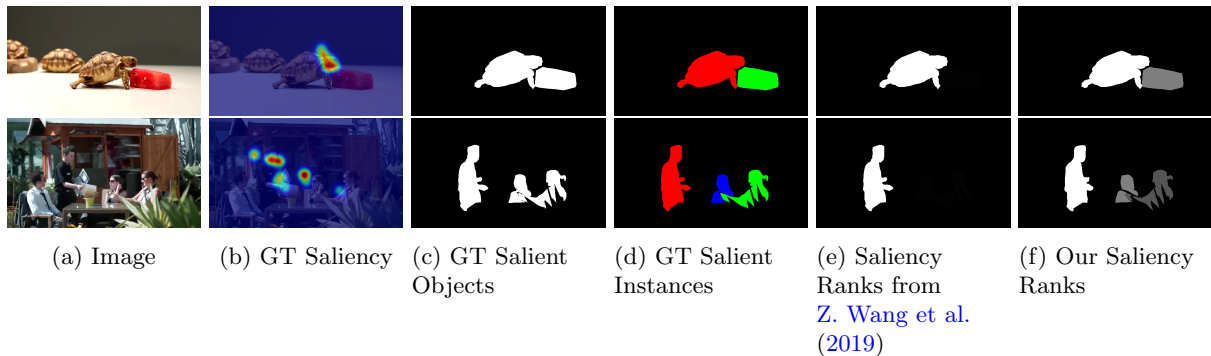


Fig. 3: Comparison between the saliency ranks generated by Z. Wang et al. (2019) and given by our annotators. (b) shows the GT saliency based on fixations. (c) shows the binary GT salient objects. (d) shows the GT salient instances. Note that the colors are used to distinguish different instances. They do not indicate the saliency ranks. While Z. Wang et al. (2019) does not generate the saliency ranks for some salient objects, our method can infer the correct salient ranks for all salient objects, which are consistent with (c) and (d).

Dataset	# of Video	# of Video Frames	Invalid Rate	Video Categories	Salient Object Types
RVSOD	364	10,513	23.9%	Sports, Movies	above 80% Human
DAVSOR (Ours)	128	17,584	0%	Daily, Animal, Vehicle, Human, Social, Sports, Art	Human, Animal Vehicle, Man-made Object

Table 1: An analysis of our proposed DAVSOR dataset, compared with RVSOD Z. Wang et al. (2019). The invalid rate is the proportion of invalid SOR videos (videos with only a single salient object) among all videos in the dataset.

Dataset	# of Video Frames	% of Salient Objects				
		1	2	3	4	5+
RVSOD	10,513	23.9	45.3	20.3	7.4	3.0
DAVSOR	17,584	-	57.8	18.8	12.5	10.9

Table 2: Statistical comparison of RVSOD Z. Wang et al. (2019) and our proposed dataset DAVSOR. The second column shows the total number of videos frames in the dataset. The third column shows the percentage of videos with a specific maximum number of salient objects in them (*i.e.*, 1, 2, 3, 4 or 5+). We can see that DAVSOR is larger in scale and more balanced compared with RVSOD Z. Wang et al. (2019).

Ren, and Sun (2016) to extract multi-scale image features. We then build a feature pyramid network Lin et al. (2017) (FPN) with multiple feature levels in a top-down manner. We further design a novel architecture with two major components:

the detection components (the black rectangle) for predicting a bounding box and a mask for each salient instance, and the ranking components (the blue and green rectangle) for predicting the saliency rank.

Specifically, the detection components consist of a region proposal network (RPN) Ren, He, Girshick, and Sun (2015) to generate region proposals for salient objects. An RoIAlign He, Gkioxari, Dollár, and Girshick (2017) layer is then used to produce the ROI features for each proposal, which are then fed into a box head to predict a bounding box and a mask head to predict the initial pixel-wise mask of each salient object. The multi-level output features from FPN are then spatially resized and fused through addition. The fused FPN features and the detected bounding boxes of each salient instance from the box head are fed into another RoIAlign layer to obtain the ROI features. We feed the output ROI features into the proposed intra-frame adaptive relation (IAR)

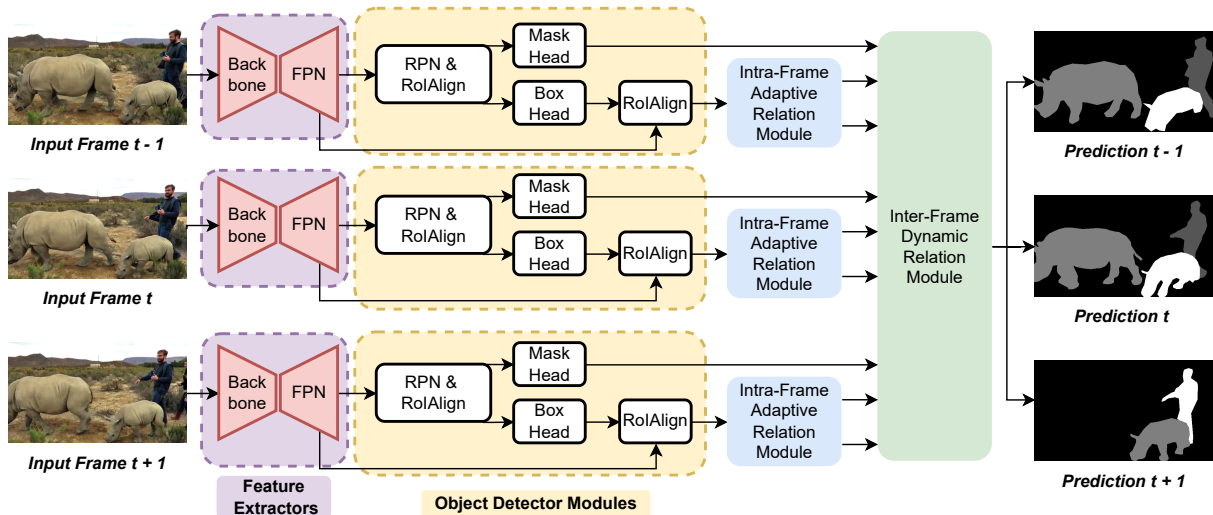


Fig. 4: The pipeline of our proposed method. In this illustration, we set the number of input frames to 3. Our method consists of four major components: the feature extractors (the red blocks), the object detector modules (the white blocks), the intra-frame adaptive relation modules (the blue blocks), and the inter-frame dynamic relation module (the green block).

module to acquire the relation features and the value features from each input frame t . Finally, the proposed IDR module takes the output relation and value features to produce the saliency score for each detected salient object. Based on the calculated saliency scores, the IDR module refines the initial mask predictions from the mask head and outputs the final saliency rank.

For the rest of this section, we discuss the IAR module (Section 4.1), the IDR module (Section 4.2), and the loss functions (Section 4.3) in detail.

4.1 The IAR Module

Our intra-frame adaptive relation (IAR) module is designed to capture the correlation among the salient objects in each individual frame. Unlike the traditional attention architecture Vaswani et al. (2017), which keeps the input, key, query, and value features on the same scale, we consider projecting the value features to a global scale in our design. Therefore, our IAR module can adaptively capture both local and global information from the key/query and value features.

Figure 5 shows the structure of our IAR module. Specifically, we take input ROI features $f_{roi} \in \mathbb{R}^{N \times C \times H \times W}$ as input, where N is the number of

detected objects from the object detector modules. C , H and W are the channel size, the height and width of the input ROI features f_{roi} . In our network, C , H and W are set to 256, 7 and 7, respectively. We first extract the key features f_k , query features f_q and the value features f_v by forwarding the ROI features f_{roi} to two individual 1×1 convolution layers. The key features f_k and the query features f_q are then reshaped into $\mathbb{R}^{N \times HW \times C}$ and $\mathbb{R}^{N \times C \times HW}$, respectively. We then multiply the reshaped key features and query features, and feed them into a scaled softmax function S to produce the intra-frame self-attention. We calculate the mean value of the value features f_v in the first dimension and reshape it into $\mathbb{R}^{HW \times C}$ to capture the global relations. The intra-frame self-attention and the reshaped f_v are then aggregated by matrix multiplication. We add these aggregated features to the original input ROI features f_{roi} to obtain the output relation features f_r . Finally, the IAR module produces two outputs, the value features f_v and the relation features f_r .

4.2 The IDR Module

Our inter-frame dynamic relation (IDR) module is designed to capture the temporal correlation of each salient object dynamically. We notice that

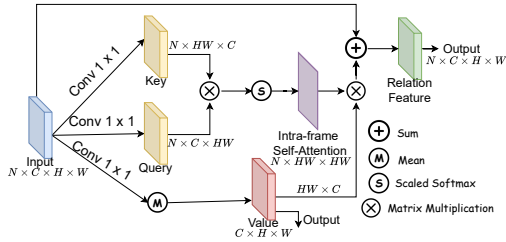


Fig. 5: Our intra-frame adaptive relation (IAR) module. It aims to learn both local and global information by projecting the key/query and the value features in different scales.

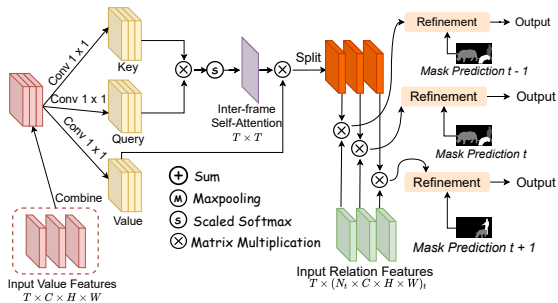


Fig. 6: Our inter-frame dynamic relation (IDR) module. In this example, we set T to 3. We use the value features that represent the global information from each video frame and calculate the inter-frame correlation among them. We then aggregate the inter-frame correlation with the intra-frame relation features frame-by-frame to produce the final features (in orange). The final features are combined with the input relation features (in green) by matrix multiplication. The refinement module takes the combined final features and the initial mask prediction as input and outputs the final saliency rank.

the saliency rank may change rapidly and dynamically at a global level (*e.g.*, the appearing and disappearing of salient objects). Hence, in our design, we use the value features with global representation for each salient object to build up the inter-frame temporal attention. By incorporating the adaptive relation with the extracted intra-frame relation, our IDR module can better utilize the spatial local and temporal global information for video salient object ranking.

Figure 6 shows the structure of our IDR module. It first takes the value features from each

frame t as input and then concatenates them into an inter-frame value features $f_v^T \in \mathbb{R}^{T \times C \times H \times W}$, where T is the number of input video frames. We then feed them into three individual 1×1 convolution layers to obtain the inter-frame key, query and value features separately. Similar to our IAR module, we obtain the inter-frame self-attention from multiplying the $T \times T$ inter-frame key and query features with proper reshaping and scaled softmax function. We then multiply the inter-frame self-attention by the value features to produce the final features (in orange). We split the combined final features into T parts and aggregate each part of them with the input relation features $f_r \in \mathbb{R}^{N_t \times C \times H \times W}$ for frame t by matrix multiplication, where N_t is the number of detected objects in frame t . We then pass the final aggregated features for each frame t to a refinement module along with the rank-agnostic mask prediction of the predictor. A fully connected layer predicts the saliency score for each detected object in the refinement module. Finally, based on the saliency score for each object, the refinement module assigns the saliency rank to the mask and outputs the final saliency rank prediction.

4.3 Loss Functions

We optimize our proposed method by jointly minimizing the loss of the salient instance boxes \mathcal{L}_{box} , salient instance masks \mathcal{L}_{mask} , classification \mathcal{L}_{cls} and saliency rank \mathcal{L}_{rank} . \mathcal{L}_{box} , \mathcal{L}_{mask} and \mathcal{L}_{cls} follow the formulations in Mask R-CNN He et al. (2017), whereas \mathcal{L}_{rank} is defined identical to the ranking loss proposed in Liu et al. (2021). The final loss function is then:

$$\mathcal{L} = \mathcal{L}_{box} + \mathcal{L}_{mask} + \mathcal{L}_{cls} + \mathcal{L}_{rank}. \quad (1)$$

5 Experiments

5.1 Implementation Details

We use ResNet-50 He et al. (2016) pre-trained on ImageNet as our backbone network. Following existing works Liu et al. (2021); Siris et al. (2020) for SOR, we first pre-train our object detector, Mask R-CNN He et al. (2017), on the MS-COCO Lin et al. (2014) 2017 training split. We follow the suggested training strategy as Liu et

Methods	Backbone	Detector	End-to-End	Fixation-Free	RVSOD		Ours (DAVSOR)	
					SA-SOR \uparrow	MAE \downarrow	SA-SOR \uparrow	MAE \downarrow
ASRNet	ResNet-101	Mask R-CNN	\times	\checkmark	0.494	0.170	0.537	0.120
Fang <i>et al.</i>	VoV-39	CenterMask	\checkmark	\checkmark	0.604	0.075	0.535	0.104
Liu	ResNet-50	Mask R-CNN	\checkmark	\checkmark	0.610	0.070	0.516	0.084
SVSNet	ResNet-50	Faster R-CNN	\times	\times	0.545	0.093	0.534	0.092
Ours	ResNet-50	Mask R-CNN	\checkmark	\checkmark	0.639	0.062	0.553	0.082
Ours	ResNet-101	Mask R-CNN	\checkmark	\checkmark	0.645	0.060	0.566	0.080

Table 3: Quantitative results on the RVSOD dataset and our proposed DAVSOR dataset. We compare our method with relevant state-of-the-art methods: ASRNet [Siris et al. \(2020\)](#), Fang *et al.* [Fang et al. \(2021\)](#), and Liu *et al.* [Liu et al. \(2021\)](#) for image salient object ranking, while SVSNet [Z. Wang et al. \(2019\)](#) and Ours for video salient object ranking. VoV-39 [Lee et al. \(2019\)](#), ResNet-50, and ResNet-101 [He et al. \(2016\)](#) are backbone networks for extracting image features. Mask R-CNN [He et al. \(2017\)](#), CenterMask [Lee and Park \(2020\)](#), and Faster R-CNN [Ren et al. \(2015\)](#) are frameworks for instance segmentation. “End-to-End” means that the method is end-to-end. “Fixation-Free” means that the method does not require fixations for training. A \checkmark and a \times indicate if the condition is satisfied or not. The best results are shown in bold.

[al. \(2021\)](#) to train our rank-agnostic Mask R-CNN: using warm-up strategy in the first 1,000 iterations and setting the total iterations to 540,000. We use stochastic gradient descent (SGD) as the optimizer for training our detector with an initial learning rate of $5e-3$, a momentum of 0.9 and a weight decay of 5×10^{-4} .

After pretraining our rank-agnostic Mask R-CNN object detector, we add the IAR module and the IDR module after the object detector and fine-tune the whole network on the two VSOR datasets: RVSOD and DAVSOR. We use Adam [Kingma and Ba \(2015\)](#) as the optimizer with a momentum of 0.9 and a weight decay of 5×10^{-4} . The base learning rate is 0.0001. The batch size is 4. The input images are resized to 640×480 . We run 10,000 and 20,000 iterations to fine-tune our network on RVSOD and DAVSOR, respectively. We also adopt random horizontal flipping as a data augmentation technique in our training. For training on DAVSOR, our model takes about 1.5 hours to converge. During inference, the test images are also first resized to 640×480 before feeding into the network and our network runs at $\sim 12fps$ on a RTX2080Ti GPU.

5.2 Evaluation Datasets

We evaluate our proposed method on two VSOR datasets: RVSOD [Z. Wang et al. \(2019\)](#) with 2,441 test video frames and our proposed dataset DAVSOR with 10,181 test video frames. All methods are trained and tested on the training/testing splits from the same dataset.

5.3 Evaluation Metrics

To statistically analyze the efficacy of our method, we use two metrics: SA-SOR [Liu et al. \(2021\)](#) and mean absolute error (MAE). SA-SOR [Liu et al. \(2021\)](#) is a segmentation-aware saliency ranking metric that has been shown to be more reliable than the original SOR [A. Islam \(2018\)](#) in terms of reflecting the correlation of the saliency ranks between the predictions and ground truth labels at the instance level. MAE is the average pixel-wise error between the predicted saliency rank and ground truth as:

$$MAE = \frac{1}{WH} \sum_{i=1}^W \sum_{j=1}^H P(i,j) - G(i,j), \quad (2)$$

where P is the predicted mask. G is the ground truth. W and H are the width and height of the ground truth.

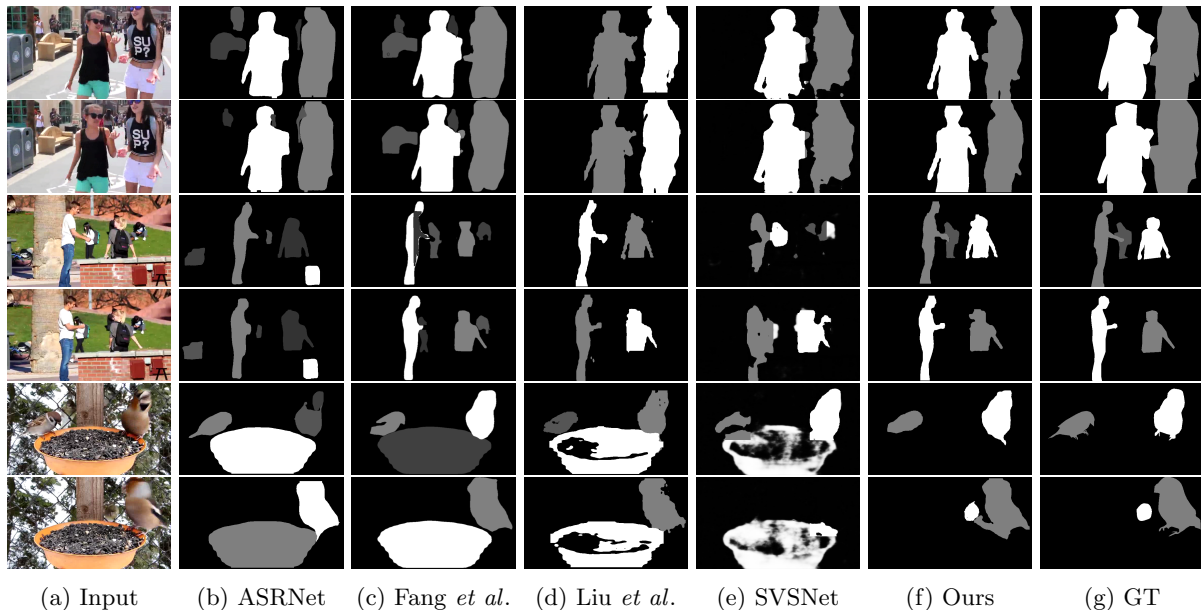


Fig. 7: Visual comparison of our method and the state-of-the-art methods on some example video frames.

5.4 Comparison with the State-of-the-arts Methods

We compare our proposed method with the state-of-the-art methods for salient object ranking, including ASRNet Siris et al. (2020), Fang et al. Fang et al. (2021), and Liu et al. Liu et al. (2021) for image salient object ranking, and SVSNet Z. Wang et al. (2019) for video salient object ranking. We use the publicly available codes of these methods with suggested configurations. Table 3 shows the comparison on two metrics: SA-SOR Liu et al. (2021) and mean absolute error (MAE). It is worth noting that although our method uses only the ResNet-50 backbone (instead of a powerful backbone and detector like Fang et al. Fang et al. (2021) or auxiliary data (e.g. fixations) like SVSNet Z. Wang et al. (2019)), it outperforms all the other methods on both metrics, especially on SA-SOR. We have also tried replacing the ResNet-50 backbone with ResNet-101 and note further performance improvement. It is obvious that a heavy backbone would likely help improve the performance, but it is not the focus of our work.

Figure 7 shows some visual comparisons. The first two, the third and the fourth, and the last two rows of video frames are selected from three

different video clips. While some existing state-of-the-art methods tend to over-detect the salient objects (e.g. ASRNet Siris et al. (2020) and Fang et al. Fang et al. (2021)), our method can correctly detect and distinguish all salient objects. Besides, we can see that our method can predict the saliency rank of different salient objects precisely, even in some very challenging scenes such as salient objects turning into non-salient objects (e.g., the middle person in the third and the fourth rows) or some objects moving very quickly leading to a rapid change of GT saliency rank (e.g., the last two rows). We attribute the superior performance of our method to the powerful relation modeling in the intra-frame and inter-frame levels.

5.5 Ablation Study

Table 4 demonstrates the effectiveness of each proposed module in our method. Note that in “Basic + IDR”, we treat the f_{roi} features from the detector as the input relational features. We observe that the “Basic” ablated model has the worst performance, showing the effectiveness of the IAR and IDR modules. We have also found that incorporating our proposed IAR module into the “Basic” ablated model helps improve the SA-SOR performance substantially more than “Basic + Self-Attention”, which we attribute to

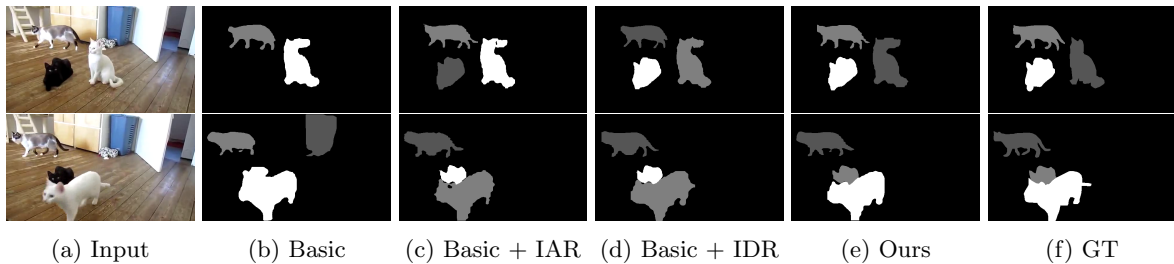


Fig. 8: A visual example of the ablation study.

Ablated Model	SA-SOR \uparrow	MAE \downarrow
Basic	0.510	0.095
Basic + Self-Attention	0.523	0.088
Basic + IAR	0.532	0.089
Basic + IDR	0.517	0.091
Ours	0.553	0.082

Table 4: Ablation study results, trained and tested on the DAVSOR dataset. “Basic” denotes the original framework with both IAR and IDR modules removed. “Basic + Self-Attention” denotes the original framework with the traditional self-attention proposed in Vaswani et al. (2017). “IAR” is the intra-frame adaptive relation module. “IDR” is the inter-frame dynamic relation module. “Ours” is the proposed full model. Best results are shown in bold.

the local-global relation modeling of our model. Further, “Basic + IAR” outperforms “Basic + IDR”, indicating that simply modeling the relationship between frames without understanding the saliency rank in static images would not help improve the performance of the proposed model much. On the other hand, as shown in the last row, our proposed full model with the IAR and IDR modules outperforms other ablated models on both metrics. It demonstrates that both the IAR and IDR modules can benefit each other in video salient object ranking.

Figure 8 shows a visual example of the component analysis. We can see that the “Basic” ablated model (b) incorrectly predicts the blue trash bin as a salient object and regards the black cat and the white cat as the same object (*i.e.*, the bottom row of Figure 8(b)) due to the insufficient

relation learning among the salient objects. Meanwhile, “Basic + IAR” (c) incorrectly predicts the white cat as the most salient object (*i.e.*, the top row of Figure 8(c)), mainly because the white cat is located at the center of the image. This indicates that only using the IAR module may overfit the spatial relation among the salient objects. Interestingly, we find that only incorporating the IDR module lets the network output the rank of the salient objects based on how they are in the previous frames (*e.g.*, the saliency rank of each object in the two input frames are identical in Figure 8(d)). While this may be a good characteristic for other vision tasks like object tracking, the performance of the model degenerates in video salient object ranking as the rank of each salient object may change across frames in VSOR. Our full network with both proposed IAR and IDR modules can extract the correct saliency rank from different video frames.

6 Limitations

Our method also has limitations. As shown in Figure 9, our method may fail in some difficult scenes, *e.g.*, scenes with a lot of objects or with very small objects. This is because our focus in this work is to learn how to rank the salient objects more accurately, instead of how to detect small objects (which is itself a separate research problem Bai, Zhang, Ding, and Ghanem (2018); J. Li et al. (2017); Noh, Bae, Lee, Seo, and Kim (2019)). As a future work, we are currently investigating ways to improve the salient object detector for video salient object ranking.

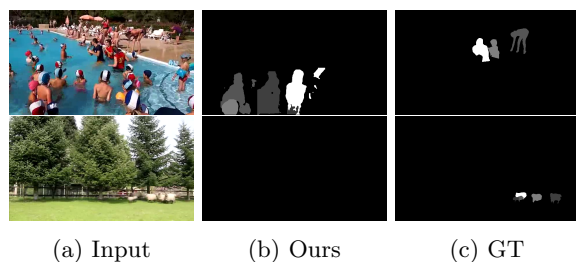


Fig. 9: Failure cases. Our method may fail to rank salient objects in some very challenging scenes that contain lots of objects (top row) or very small salient objects (bottom row).

7 Conclusion

In this paper, we have revisited the video salient object ranking problem. We have made the following contributions. First, we have created DAVSOR, a large-scale and challenging video salient object ranking dataset with 17,584 video frames and corresponding human-annotated saliency rank masks. This dataset includes various types of videos and salient objects. Second, we have proposed a new end-to-end method for video salient object ranking, which includes two novel modules: an intra-frame adaptive relation (IAR) module to model the saliency degrees among different objects on an intra-frame level, and an inter-frame dynamic relation module (IDR) to model the saliency ranks across different frames. Finally, we have conducted comprehensive experiments to demonstrate that the proposed method outperforms existing state-of-the-art models on the video salient object ranking task.

References

- A. Islam, N.D.B.B., M. Kalash (2018). Revisiting salient object detection: Simultaneous detection, ranking, and subitizing of multiple salient objects. *Cvpr*.
- Bai, Y., Zhang, Y., Ding, M., Ghanem, B. (2018). Sod-mtgan: Small object detection via multi-task generative adversarial network. *Eccv*.
- Chen, C., Li, S., Wang, Y., Qin, H., Hao, A. (2017). Video saliency detection via spatial-temporal fusion and low-rank coherency diffusion. *IEEE Transactions on Image Processing*, 26(7), 3156–3170.
- Fan, D.-P., Wang, W., Cheng, M.-M., Shen, J. (2019). Shifting more attention to video salient object detection. *Cvpr* (pp. 8554–8564).
- Fang, H., Zhang, D., Zhang, Y., Chen, M., Li, J., Hu, Y., ... He, X. (2021). Salient Object Ranking With Position-Preserved Attention. *Iccv*.
- Gu, Y., Wang, L., Wang, Z., Liu, Y., Cheng, M.-M., Lu, S.-P. (2020). Pyramid constrained self-attention network for fast video salient object detection. *Aaai*.
- Guo, C., Ma, Q., Zhang, L. (2008). Spatio-temporal saliency detection using phase spectrum of quaternion fourier transform. *Cvpr*.
- Guo, F., Wang, W., Shen, J., Shao, L., Yang, J., Tao, D., Tang, Y.Y. (2017). Video saliency detection using object proposals. *IEEE transactions on cybernetics*, 48(11), 3159–3170.
- He, K., Gkioxari, G., Dollár, P., Girshick, R. (2017). Mask r-cnn. *Iccv*.
- He, K., Zhang, X., Ren, S., Sun, J. (2016). Deep residual learning for image recognition. *Cvpr* (pp. 770–778).
- Kingma, D.P., & Ba, J. (2015). Adam: A method for stochastic optimization. *ICLR*.
- Koch, C., & Ullman, S. (1987). Shifts in selective visual attention: towards the underlying neural circuitry. *Matters of intelligence* (pp. 115–141). Springer.
- Lee, Y., Hwang, J.-w., Lee, S., Bae, Y., Park, J. (2019). An energy and gpu-computation efficient backbone network for real-time object detection. *Cvpr workshops*.

- Lee, Y., & Park, J. (2020). Centermask: Real-time anchor-free instance segmentation. *Cvpr*.
- Li, G., Xie, Y., Wei, T., Wang, K., Lin, L. (2018). Flow guided recurrent neural encoder for video salient object detection. *Cvpr*.
- Li, H., Chen, G., Li, G., Yu, Y. (2019). Motion guided attention for video salient object detection. *Iccv* (pp. 7274–7283).
- Li, J., Liang, X., Wei, Y., Xu, T., Feng, J., Yan, S. (2017). Perceptual generative adversarial networks for small object detection. *Cvpr* (pp. 1222–1230).
- Li, Z., Qin, S., Itti, L. (2011). Visual attention guided bit allocation in video compression. *Image and Vision Computing*, 29(1), 1–14.
- Lin, T.-Y., Dollár, P., Girshick, R., He, K., Hariharan, B., Belongie, S. (2017). Feature pyramid networks for object detection. *Cvpr* (pp. 2117–2125).
- Lin, T.-Y., Maire, M., Belongie, S., Hays, J., Perona, P., Ramanan, D., ... Zitnick, C.L. (2014). Microsoft coco: Common objects in context. *Eccv* (pp. 740–755).
- Liu, N., Li, L., Zhao, W., Han, J., Shao, L. (2021). Instance-level relative saliency ranking with graph reasoning. *IEEE TPAMI*.
- Mathe, S., & Sminchisescu, C. (2014). Actions in the eye: Dynamic gaze datasets and learnt saliency models for visual recognition. *IEEE TPAMI*, 37(7), 1408–1424.
- Noh, J., Bae, W., Lee, W., Seo, J., Kim, G. (2019). Better to follow, follow to be better: Towards precise supervision of feature super-resolution for small object detection. *Iccv*.
- Ren, S., Han, C., Yang, X., Han, G., He, S. (2020). Tenet: Triple excitation network for video salient object detection. *Eccv* (pp. 212–228).
- Ren, S., He, K., Girshick, R., Sun, J. (2015). Faster r-cnn: Towards real-time object detection with region proposal networks. *NeurIPS*.
- Siris, A., Jiao, J., Tam, G.K., Xie, X., Lau, R.W. (2020, June). Inferring attention shift ranks of objects for image saliency. *Cvpr*.
- Song, H., Wang, W., Zhao, S., Shen, J., Lam, K.-M. (2018). Pyramid dilated deeper convlstm for video salient object detection. *Eccv*.
- Vaswani, A., Shazeer, N., Parmar, N., Uszkoreit, J., Jones, L., Gomez, A.N., ... Polosukhin, I. (2017). Attention is all you need. *Neurips*.
- Wang, W., Shen, J., Shao, L. (2015). Consistent video saliency using local gradient flow optimization and global refinement. *IEEE Transactions on Image Processing*, 24(11), 4185–4196.
- Wang, W., Shen, J., Shao, L. (2017). Video salient object detection via fully convolutional networks. *IEEE Transactions on Image Processing*, 27(1), 38–49.
- Wang, W., Shen, J., Xie, J., Cheng, M.-M., Ling, H., Borji, A. (2019). Revisiting video saliency prediction in the deep learning era. *IEEE transactions on pattern analysis and machine intelligence*, 43(1), 220–237.
- Wang, Z., Yan, X., Han, Y., Sun, M. (2019). Ranking video salient object detection. *Acm mm* (pp. 873–881).
- Xingjian, S., Chen, Z., Wang, H., Yeung, D.-Y., Wong, W.-K., Woo, W.-c. (2015). Convolutional lstm network: A machine learning approach for precipitation nowcasting. *Neurips* (pp. 802–810).
- Yao, T., Pan, Y., Li, Y., Mei, T. (2018). Exploring visual relationship for image captioning. *Eccv* (pp. 684–699).

Zhang, J., Sclaroff, S., Lin, Z., Shen, X., Price, B., Mech, R. (2015). Minimum barrier salient object detection at 80 fps. *Iccv* (pp. 1404–1412).

Zhang, M., Liu, J., Wang, Y., Piao, Y., Yao, S., Ji, W., ... Luo, Z. (2021). Dynamic context-sensitive filtering network for video salient object detection. *Iccv*.

Author Biographies

Jiaying Lin is currently a PhD student in Computer Science at City University of Hong Kong. He received the B.Eng. degree in Computer Science and Technology from South China University and Technology in 2019. His research interests include computer vision and computer graphics.

Huankang Guan received his B.Eng. degree in Computer Science from Wuhan University. He is currently a PhD student in Computer Science at City University of Hong Kong. His research interests include computer vision and deep learning.

Rynson W.H. Lau received his Ph.D. degree from University of Cambridge. He has been on the faculty of Durham University, and City University of Hong Kong.

Rynson serves on the Editorial Board of International Journal of Computer Vision (IJCV). He has served as the Guest Editor of a number of journal special issues, including ACM Trans. on Internet Technology, IEEE Trans. on Multimedia, IEEE Trans. on Visualization and Computer Graphics, and IEEE Computer Graphics & Applications. He has also served in the committee of a number of conferences, including Program Co-chair of ACM VRST 2004, ACM MTDL 2009, IEEE U-Media 2010, and Conference Co-chair of CASA 2005, ACM VRST 2005, ACM MDI 2009, ACM VRST 2014. Rynson's research interests include computer graphics and computer vision.